Supplemental Material

Real-time investigation of primary ship engine emissions by vacuum resonanceenhanced multiphoton ionization highresolution Orbitrap mass spectrometry

Paul Kösling^{1,2,3}, Christopher P. Rüger^{1,2*}, Julian Schade^{1,2,3}, Sven Ehlert⁴, Uwe Etzien⁵, Anton N. Kozhinov⁶, Yury O. Tsybin⁶, Martin Rigler⁷, Thomas Adam³, Andreas Walte⁴, Bert Buchholz⁵, and Ralf Zimmermann^{1,2,8}

- 1 Joint Mass Spectrometry Centre (JMSC)/Chair of Analytical Chemistry, University of Rostock, 18059 Rostock, Germany
- 2 Department Life, Light & Matter (LLM), University of Rostock, 18059 Rostock, Germany
- 3 Institute of Chemistry and Environmental Engineering, University of the Bundeswehr Munich, 85579 Neubiberg, Germany
- 4 Photonion GmbH, 19061 Schwerin, Germany
- 5 Chair of Piston Machines and Internal Combustion Engines, University of Rostock, 18059 Rostock, Germany
- 6 Spectroswiss, 1015 Lausanne, Switzerland
- 7 Aerosol d.o.o., SI-1000 Ljubljana, Slovenia
- 8 Joint Mass Spectrometry Centre, Cooperation Group "Comprehensive Molecular Analytics", Helmholtz Zentrum Muenchen, Neuherberg, D-85764, Germany

Keywords: ship emissions, online measurement, scrubber, heavy fuel oil, laser photoionization

^{* -} corresponding author: christopher.rueger@uni-rostock

Table S1: Estimated Limits of Detection (LOD) for species from a standard gas mixture (Benzene, Toluene, Xylene, Trimethylbenzene). LODs are calculated for mass spectra averaged over 1, 10 and 60 s, respectively. For calculation, the signal-to-noise ratio (S/N) of the averaged mass spectra within mentioned time frames is used, assuming a minimal S/N of 3.

Figure S1: a) PhotOrbi inside the control room directly next to the research ship diesel engine. The heated sampling line entering the engine compartment is depicted at the left. b) Simplified setup for the emission gas sampling. The ship's diesel exhaust gas is diluted with nitrogen and subsequently hot-filtered to remove the particle phase. The dilution ratio is controlled and monitored by two flow controllers. Heating hoses acting as transfer and sampling lines ensure a gas temperature of at least 250 °C to prevent condensation. A deactivated fused-silica capillary guides the diluted gas phase into the Orbitrap mass spectrometer. Most of the sample raw gas is not introduced in the mass spectrometer and is subjected to a waste stream after the dilution. Here, the dispensable volume is guided through a water bath (5 °C) and a filter cartridge (silica gel, active carbon) before the flow controller and membrane pump. Despite sensitive state-of-the-art electronics and an excimer laser system, the PhotOrbi could be brought via a small truck to the research ship diesel emission site and restarted without any problems. After overnight pumping (mass analyzer pressure: ~4e-10 mbar), the system was ready for operation, and the general response was tested by measurements of a gas standard (benzene, toluene, xylene, trimethylbenzene) (Figure S2, Supporting Information).

Figure S2: Exemplary mass spectrum of an averaged 1 s PhotOrbi measurement of the gas standard (Benzene, Toluene, Xylene, Trimethylbenzene). The measurement is evaluated for limit of detection estimation. Species and corresponding limits are labeled.

Figure S3: Error histogram for the elemental composition attribution of the engine start up (fuel shift from diesel to heavy fuel oil) is shown. A root mean square error (RSME) of 0.18 ppm with 380 species could be achieved.

Figure S4: Total Ion Current (TIC) for engine start-up. The engine is operated about 200 s with diesel fuel for heating up the engine, resulting in relative low emissions. After 200 s the diesel fuel is changed for a heavy fuel oil as feed, leading to a rapid increase in emission and, thus, observed mass spectrometric response.

Figure S5: a) Histogram of the mass position data shown in Figure 2c) (main body). A symmetric Gaussian distribution centered very close to the theoretical value and an FWHM of <0.4 ppm. b) Histogram of the resolution data shown in Figure 2d) (main body). A Gaussian behavior, centered at R ~143k, with very low asymmetry towards higher values can be observed.

Figure S6: a) Time-resolved scatter visualization of the ratio of the highest to the lowest abundance peak-picked signal, color-coded according to total ion current (TIC) as a measure of the single-scan dynamic range. As the ion (charge) capacity of the Orbitrap mass analyzer is not reached, naturally, a strong positive correlation with the TIC is found. b) Exemplary profile mass spectrometric expanded view to the isotopic fine structure profile of $C_{16}H_{10}^+$ of the averaged mass spectrum (~2000 s). The isotopologues can be fully (baseline) resolved from other signals, and low deviations for the intensity distribution as well as exact m/z location are observed, allowing further validation of the attributed elemental compositions.

Figure S7: Time-resolved visualization of the deviation of the fine isotopic abundances (13 C pattern) as difference between experimental and theoretical value (blue: $1x^{13}$ C and red: $2x^{13}$ C).

Figure S8: (1) Exemplary scenario for the identification of an unknown species at m/z 202.0777. Assuming limited knowledge on the sample. (2) Creating list of possible species based on peak position and error boarder (here, a tolerance window of 10 ppm is chosen). Peak cannot be assigned to one specific species, therefore cross validation via isotopic pattern is used. (3) Calculation of the theoretical isotopic pattern. (4) Determination of experimental error boundaries and comparison to the theoretical values calculated in (3). Here, $C_{16}H_{10}$ is the only possible attribution.

Figure S9: DBE distribution (summed abundance of the respective molecular attributions) from the averaged HFO spectra over 5 min. The DBE values ranging from 4 to 17, with an overall maximum at DBE 10 (peri-condensed 4-ring PAHs). The strongest contribution of heteroatom-containing PAHs has been found for DBE 9, e.g., alkylated-derivatives of dibenzothiophene. Superimposed to the pattern at DBE 4, 7, 10 (benzene and two- and cate-three-ring PAHs), DBE 9 and 12 are spiking (ortho/peri-fused three and four-ring PAHs).

Figure S10: Mass spectra for various fuels (diesel, HFO, HFO after scrubber, VLSFO) are displayed in the mass range of 0 to 500 m/z averaged over 5 minutes. HFO and VLSFO exhaust show a strong pattern due to alkylated species and one order of magnitude higher signal intensity compared to diesel. Dominating species for diesel are pyrene (m/z 202) and phenanthrene/anthracene (m/z 178). Compared to diesel fuel also oxidized as well as sulfur species can be found. Diesel, VLSFO and HFO were sampled with an initial exhaust gas temperature of about 300 °C, HFO after scrubber with a temperature of about 30 °C.

Figure S11: Compound class distribution of the diesel emissions. The displayed data are average chemical speciation from 5 min (540 scans) of stable emission conditions at 20 kW load.

Figure S12: Compound class distribution of the heavy fuel oil emissions without scrubber. The displayed data are average chemical speciation from 5 min (540 scans) of stable emission conditions at 20 kW load.

Figure S13: Compound class distribution of the heavy fuel oil emissions with scrubber. The displayed data are average chemical speciation from 5 min (540 scans) of stable emission conditions at 20 kW load.

Figure S14: Compound class distribution of the very low sulfur fuel oil. The displayed data are average chemical speciation from 5 min (540 scans) of stable emission conditions at 20 kW load.

Figure S15: Kendrick mass defect plots for the mass increment CH₂. Compound classes are color-coded (blue – CH-, red – CHO-, and yellow – CHS-class). Please note that for visualization the size of the CHO- and CHS-class compounds is increased by a factor of 10. CHS-class relative contribution nicely correlates with fuel sulphur content (FSC). No significant effect was found comparing primary HFO gas emissions and HFO emissions after wet-scrubber exhaust gas treatment. Important for regulatory bodies, the VLSFO, despite being a low sulphur feed, exhibits a strong profile of unsaturated aromatic constituents with high mass defects. The nature of these alarming compounds released from an IMO 2020 permitted fuel can most likely be traced back to the cycle-oil (a cheap by-product in petroleum refining) content of the VLSFO.

Figure S16: Extracted time-resolved traces for the CH- and CHO-class as well as the exemplary attributed elemental compositions $C_{16}H_{10}O_1$ (DBE 10) and $C_{15}H_{10}S_1$ (DBE 11) for the transmission from a) diesel to heavy fuel oil (HFO), with a stabilization at about 1,000 s, and b) diesel to very low sulfur fuel oil, stabilizing at roughly 1,200 s. For both cases, an overall increase for all traces is noticeable after change from distillate fuel towards a heavier feed.

Table S1: Estimated Limits of Detection (LOD) for species from a standard gas mixture (Benzene, Toluene, Xylene, Trimethylbenzene). LODs are calculated for mass spectra averaged over 1, 10 and 60 s, respectively. For calculation, the signal-to-noise ratio (S/N) of the averaged mass spectra within mentioned time frames is used, assuming a minimal S/N of 3.

m/z	LOD v-ppm Averaged: 1 s	LOD v-ppm Averaged: 10 s	LOD v-ppm Averaged: 60 s
78	2.2880	0.7562	0.3456
92	1.7273	0.5165	0.2560
106	0.3597	0.1106	0.0513
120	0.5720	0.1753	0.0843

The setup for adjusting initial system parameters via a standard gas mixture (benzene, toluene, xylene, 1,2,4-trimethylbenzene, concentration of each compound: 10 v-ppm)1 can also be used for determining the limits of detections (LODs) for these reference four aromatic compounds as a figure of merit not discussed so far. As briefly addressed for the CHS-class compounds, the REMPI signal response is not only given by the gas density (concentration) but also strongly depends on the ionization cross section and, thus, on the deployed laser wavelength as well as on the number of photons (laser fluency). Generally, REMPI is a very soft ionization scheme, preserving molecular information. Nonetheless, depending on the molecular structure, a certain fragmentation can appear. This fragmentation is also dependent on laser fluence. Hence, determining the optimal LOD is a balancing act between sensitivity and softness of the ionization. For rather stable PAH cores, only minimal fragmentation can be found, even for high laser fluencies. Still, highly alkylated derivatives can easily cleave side chains (dealkylation), forming even-electron fragment species, addressed later in more detail in the fuel discussion section. Cross-section dependency will lead to LODs with several orders of magnitude in difference. For the given standards, LODs assuming a minimal S/N of 3 are summarized in Table S1. LOD will also depend on the number of averaged spectrometric information (co-added time-domain transients). Thus, LODs have been calculated for 1 s, 10 s, and 1 min, for 2, 18, and 108 scans, respectively, by the S/N ratios from the corresponding averaged mass spectra. With this approach, LODs ranging from ppm down to ppb are achieved. REMPI cross-sections for PAHs with a higher number of annulated rings (higher DBE values) have been reported to be significantly higher than for the DBE 4 species given in the gas standard.^{2,3} Hence, a low v-ppb sensitivity for these compounds, e.g., dominating the emission spectrum of the bunker fuel feeds, can fairly be assumed, particularly for the feed fuel comparison discussed below utilizing a 5 min response from stabilized engine emissions.

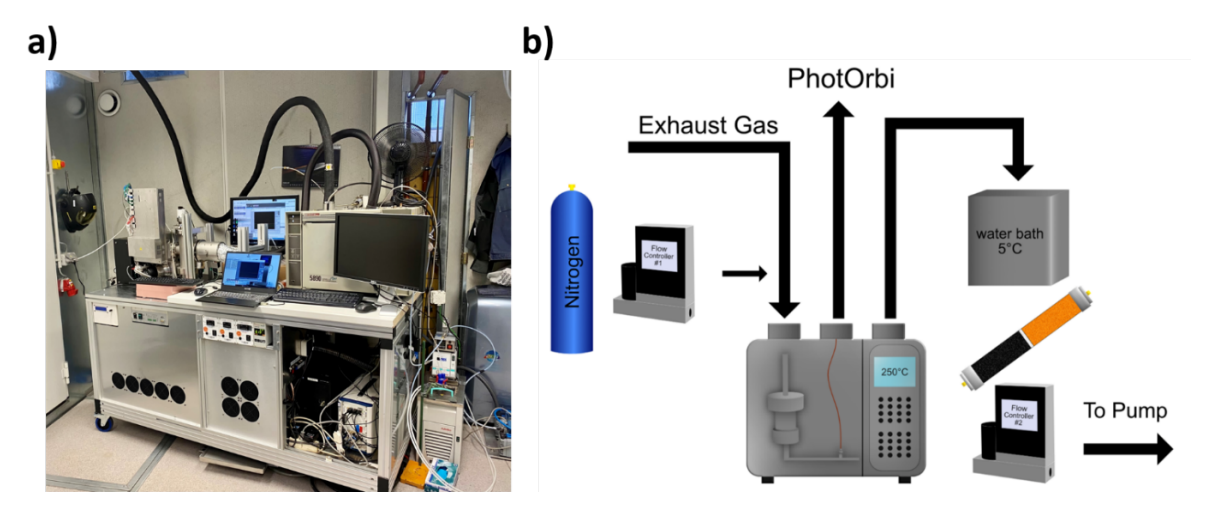


Figure S1: a) *PhotOrbi* inside the control room directly next to the research ship diesel engine. The heated sampling line entering the engine compartment is depicted at the left. b) Simplified setup for the emission gas sampling. The ship's diesel exhaust gas is diluted with nitrogen and subsequently hot-filtered to remove the particle phase. The dilution ratio is controlled and monitored by two flow controllers. Heating hoses acting as transfer and sampling lines ensure a gas temperature of at least 250 °C to prevent condensation. A deactivated fused-silica capillary guides the diluted gas phase into the Orbitrap mass spectrometer. Most of the sample raw gas is not introduced in the mass spectrometer and is subjected to a waste stream after the dilution. Here, the dispensable volume is guided through a water bath (5 °C) and a filter cartridge (silica gel, active carbon) before the flow controller and membrane pump.

Despite sensitive state-of-the-art electronics and an excimer laser system, the *PhotOrbi* could be brought via a small truck to the research ship diesel emission site and restarted without any problems. After overnight pumping (mass analyzer pressure: ~4e-10 mbar), the system was ready for operation, and the general response was tested by measurements of a gas standard (benzene, toluene, xylene, trimethylbenzene) (Figure S2, Supporting Information).

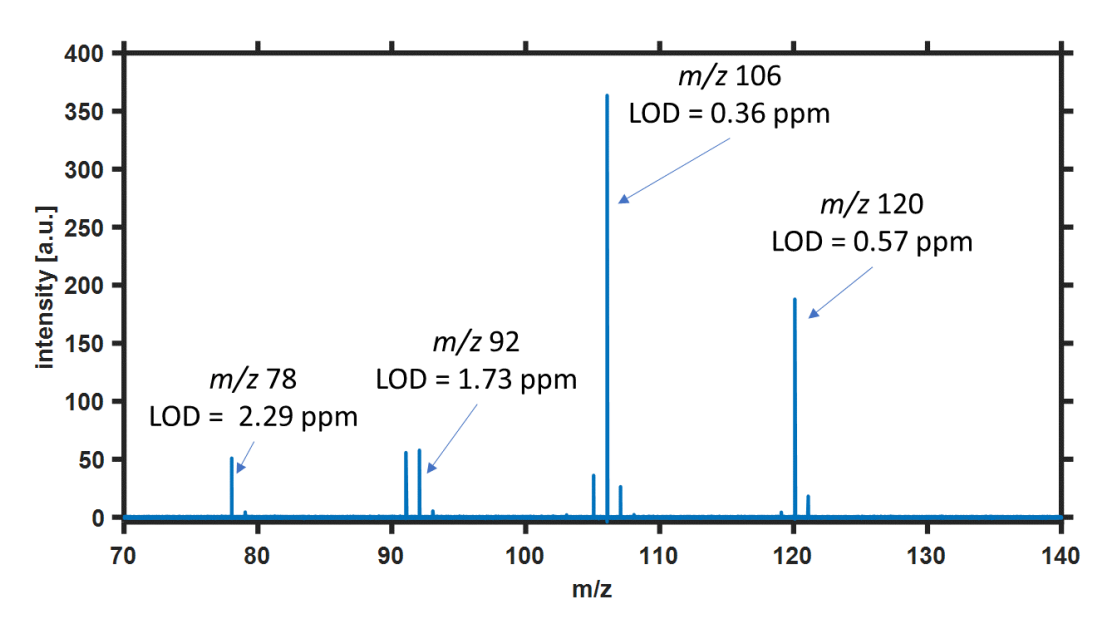


Figure S2: Exemplary mass spectrum of an averaged 1 s PhotOrbi measurement of the gas standard (Benzene, Toluene, Xylene, Trimethylbenzene). The measurement is evaluated for limit of detection estimation. Species and corresponding limits are labeled.

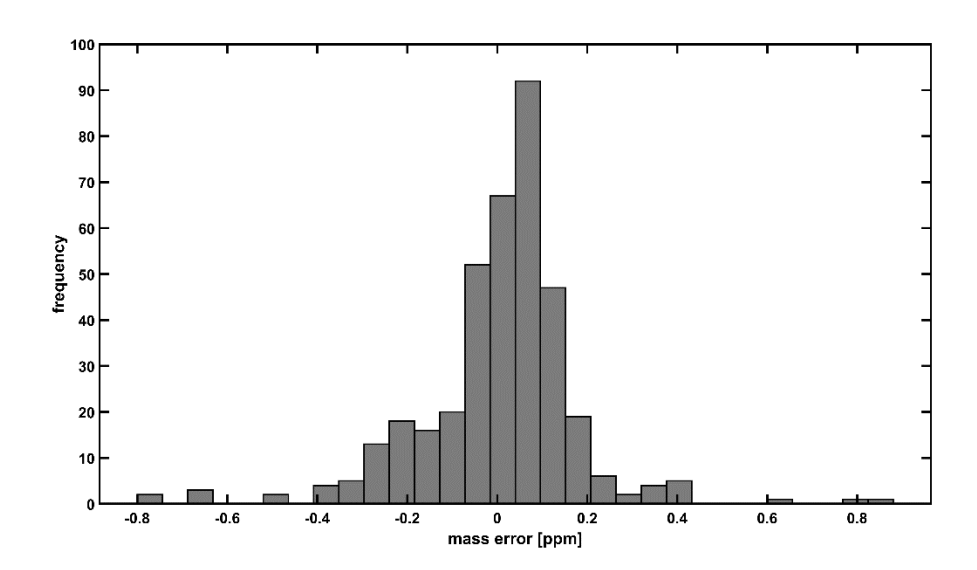


Figure S3: Error histogram for the elemental composition attribution of the engine start up (fuel shift from diesel to heavy fuel oil) is shown. A root mean square error (RSME) of 0.18 ppm with 380 species could be achieved.

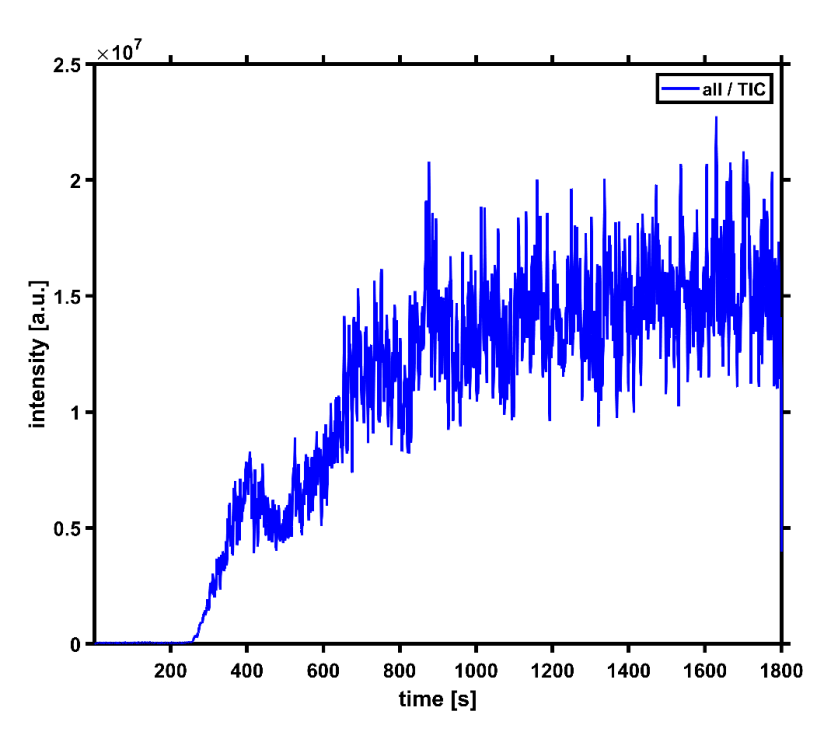


Figure S4: Total Ion Current (TIC) for engine start-up. The engine is operated about 200 s with diesel fuel for heating up the engine, resulting in relative low emissions. After 200 s the diesel fuel is changed for a heavy fuel oil as feed, leading to a rapid increase in emission and, thus, observed mass spectrometric response.

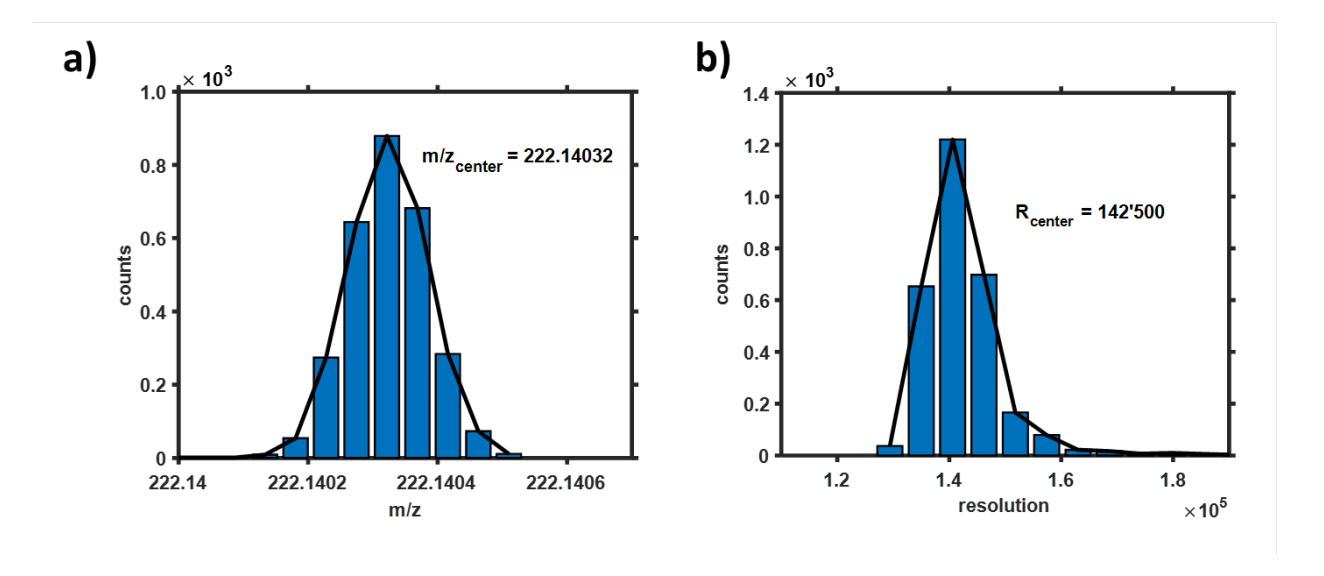


Figure S5: a) Histogram of the mass position data shown in Figure 2c) (Article). A symmetric Gaussian distribution centered very close to the theoretical value and an FWHM of <0.4 ppm. b) Histogram of the resolution data shown in 2d) (Article). A Gaussian behavior, centered at R ~143k, with very low asymmetry towards higher values can be observed.

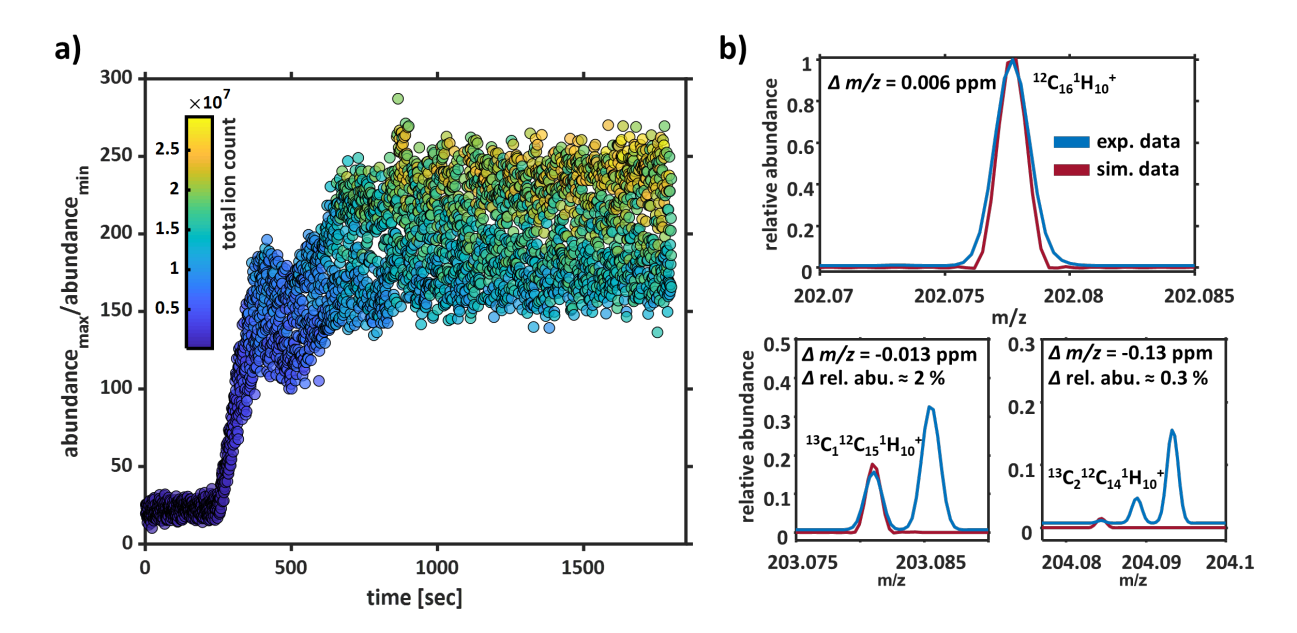


Figure S6: a) Time-resolved scatter visualization of the ratio of the highest to the lowest abundance peak-picked signal, color-coded according to total ion current (TIC) as a measure of the single-scan dynamic range. As the ion (charge) capacity of the Orbitrap mass analyzer is not reached, naturally, a strong positive correlation with the TIC is found. b) Exemplary profile mass spectrometric expanded view to the isotopic fine structure profile of $C_{16}H_{10}^+$ of the averaged mass spectrum (~2000 s). The isotopologues can be fully (baseline) resolved from other signals, and low deviations for the intensity distribution as well as exact m/z location are observed, allowing further validation of the attributed elemental compositions.

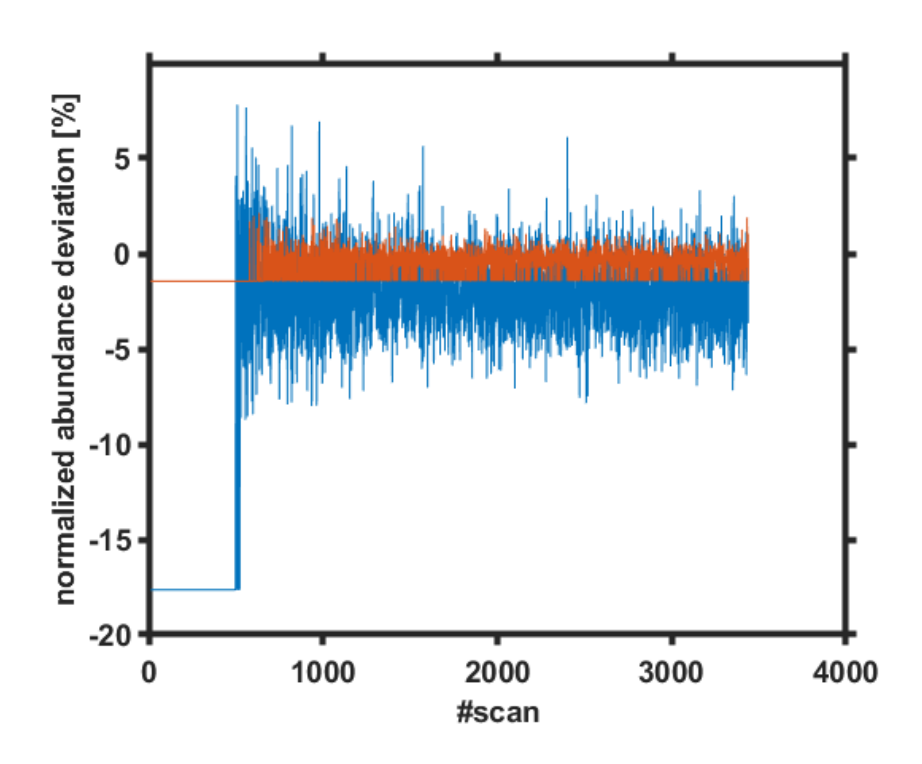


Figure S7: Time-resolved visualization of the deviation of the fine isotopic abundances (13 C pattern) as difference between experimental and theoretical value (blue: 1x 13 C and red: 2x 13 C).

1 Validation via isotopologues - Workflow

- limited knowledge on sample (elements: CHNOS)
 - peak found at m/z (experimental) 202.0777

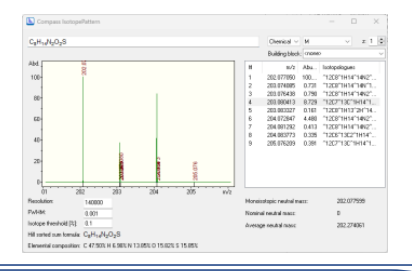
2

- creating list of possible species (±10 ppm)
- elemental boundaries: $C_{1-\infty}H_{0-\infty}S_{0-10}O_{0-20}N_{0-10}$
- possible species found: C₈H₁₄N₂O₂S₁
- cross validation via isotopic pattern



3

- Iterate through species, e.g., C₈H₁₄N₂O₂S₁
- theoretical isotopic ratio via calculation tool (here Bruker Compass IsotopePattern)



4 • identification of the isotopologues via abundance pattern (monoisotopic signal highest abundance) and delta m/z

- determine experimental error boundaries for the isotope distribution via standard deviation of scan-by-scan data \rightarrow 1^{st 13}C isotopologue: 2.04 %, 2^{nd 13}C isotopologue: 0.44 %,
- relative abundance of species $C_8H_{14}N_2O_2S_1$ ¹³C isotopologues (8.73 %, 0.34 %, indicated as red line × in bar plot) is not within the error boundary (15.60 ± 2.04, 1.29 ± 0.44)
- C₈H₁₄N₂O₂S₁ is presumably **not the detected** species
- further species: $C_{16}H_{14}$ (17.31 %, 1.40 %)/ $C_6H_{12}N_5O_1S_1$ (6.53 %, 0.18 %)
- solely $C_{16}H_{14}$ falls within the error margins \rightarrow successful validation via isotopologues

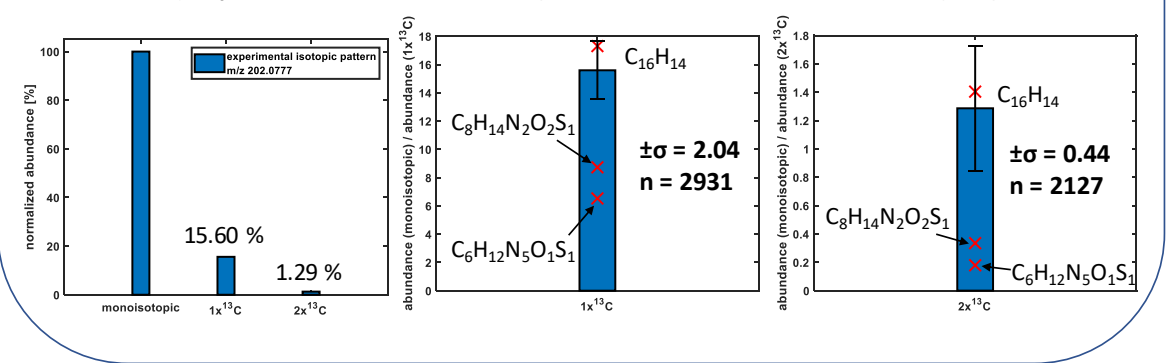


Figure S8: (1) Exemplary scenario for the identification of an unknown species at m/z 202.0777. Assuming limited knowledge on the sample. (2) Creating list of possible species based on peak position and error boarder (here, a tolerance window of 10 ppm is chosen). Peak cannot be assigned to one specific species, therefore cross validation via isotopic pattern is used. (3) Calculation of the theoretical isotopic pattern. (4) Determination of experimental error boundaries and comparison to the theoretical values calculated in (3). Here, $C_{16}H_{10}$ is the only possible attribution.

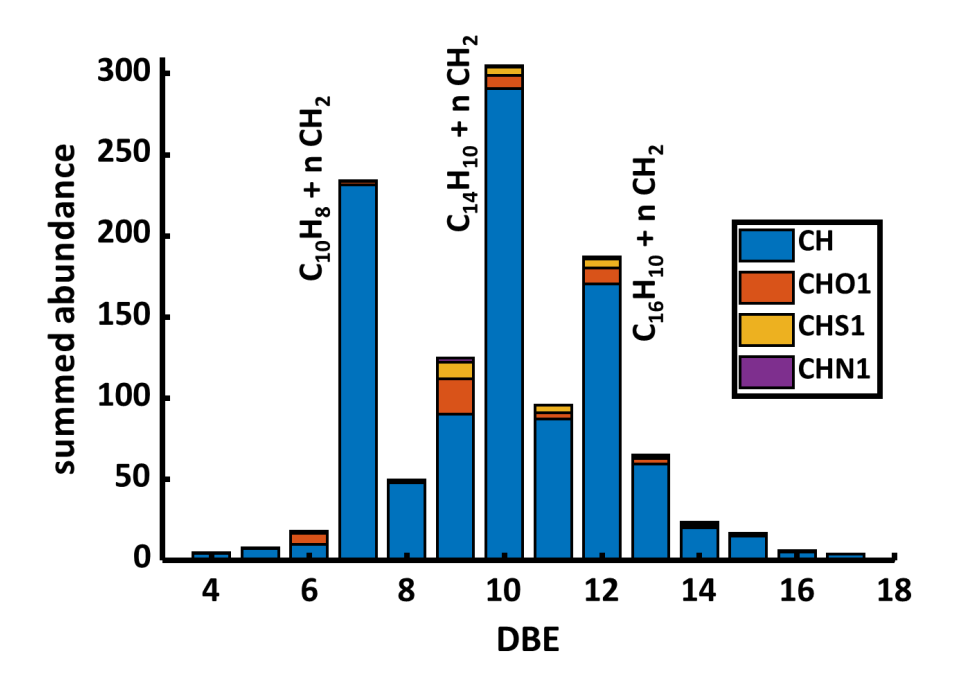


Figure S9: DBE distribution (summed abundance of the respective molecular attributions) from the averaged HFO spectra over 5 min. The DBE values ranging from 4 to 17, with an overall maximum at DBE 10 (peri-condensed 4-ring PAHs). The strongest contribution of heteroatom-containing PAHs has been found for DBE 9, e.g., alkylated-derivatives of dibenzothiophene. Superimposed to the pattern at DBE 4, 7, 10 (benzene and two- and cate-three-ring PAHs), DBE 9 and 12 are spiking (ortho/peri-fused three and four-ring PAHs).

The [1+1] REMPI process (one-color two-photon REMPI) primarily addresses intermediate excited states of aromatic compounds, leading to an efficient and selective ionization of those unsaturated constituents. 6,4,5 . This behavior can also be depicted from the DBE distribution of the attributed molecular formula, given in Figure S8. This observation can analogously be made for the other feed fuel types (Figure 3). For HFO DBE values ranging from 4 to approx. 17 could be found, where the lowest DBE value is given by alkylated derivatives of the one-core aromatic structure of benzene ($C_6H_6 + n \times CH_2$, n - non-negative integer) as the smallest CH-class compound following the Hückel's rule for aromatic properties ($4n + 2\pi$ electrons, n – non negative integer). Lower DBE values can be found for cyclic heteroatom compounds, such as thiophene (C_4H_4S , DBE 3) or furan (C_4H_4O , DBE 3), theoretically detectable but not observed in this study. Moreover, strong contributions in the DBE distribution can be found for DBE 7 and 10, presumably naphthalene (cata-condensed two-ring PAH) and anthracene/phenanthrene (cata-condensed, 3-ring PAHs) as well as DBE 9 and 12, presumably fluorene/acenaphthylene (peri-condensed 3-ring PAHs) and pyrene/fluoranthene (peri-condensed 4-ring PAHs), respectively. The superimposed pattern with a DBE spacing results from the annulation of

benzene units to the growing PAH cores and is commonly found as a leading structural motive in *petroleomics*.^{7,8} For the CHO₁- and CHS₁-class, the highest contribution has been found for DBE 9, *e.g.*, dibenzo-furan -thiophen structures. REMPI is selectively exploiting the aromatic portion of the chemical space as a crucial fraction with respect to unburned/partially burned fuel (*petrogenic*) and/or the formation of combustion products and soot precursory (*pyrogenic*).

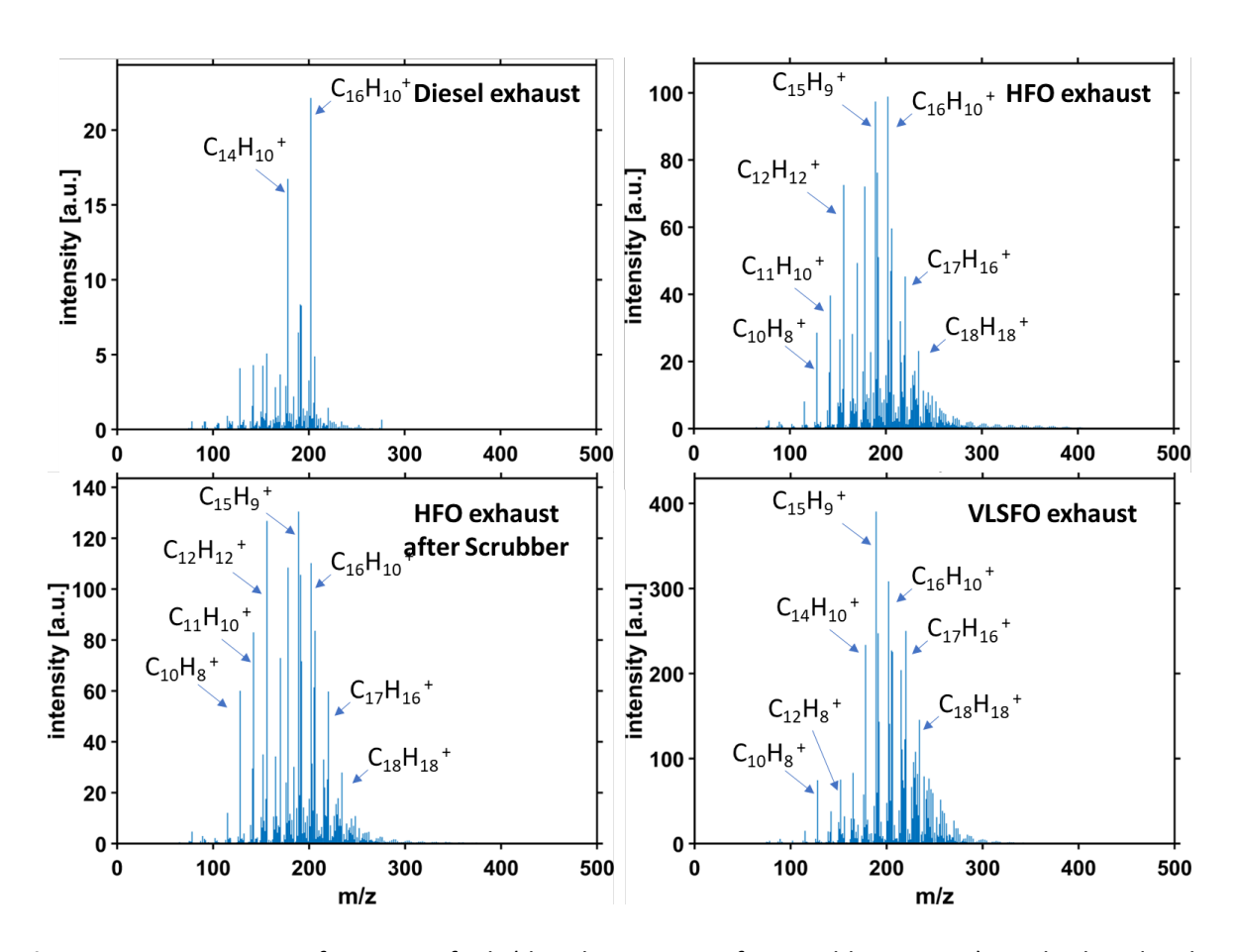


Figure S10: Mass spectra for various fuels (diesel, HFO, HFO after scrubber, VLSFO) are displayed in the mass range of 0 to 500 m/z averaged over 5 minutes. HFO and VLSFO exhaust show a strong pattern due to alkylated species and one order of magnitude higher signal intensity compared to diesel. Dominating species for diesel are pyrene (m/z 202) and phenanthrene/anthracene (m/z 178). Compared to diesel fuel also oxidized as well as sulfur species can be found. Diesel, VLSFO and HFO were sampled with an initial exhaust gas temperature of about 300 °C, HFO after scrubber with a temperature of about 30 °C.

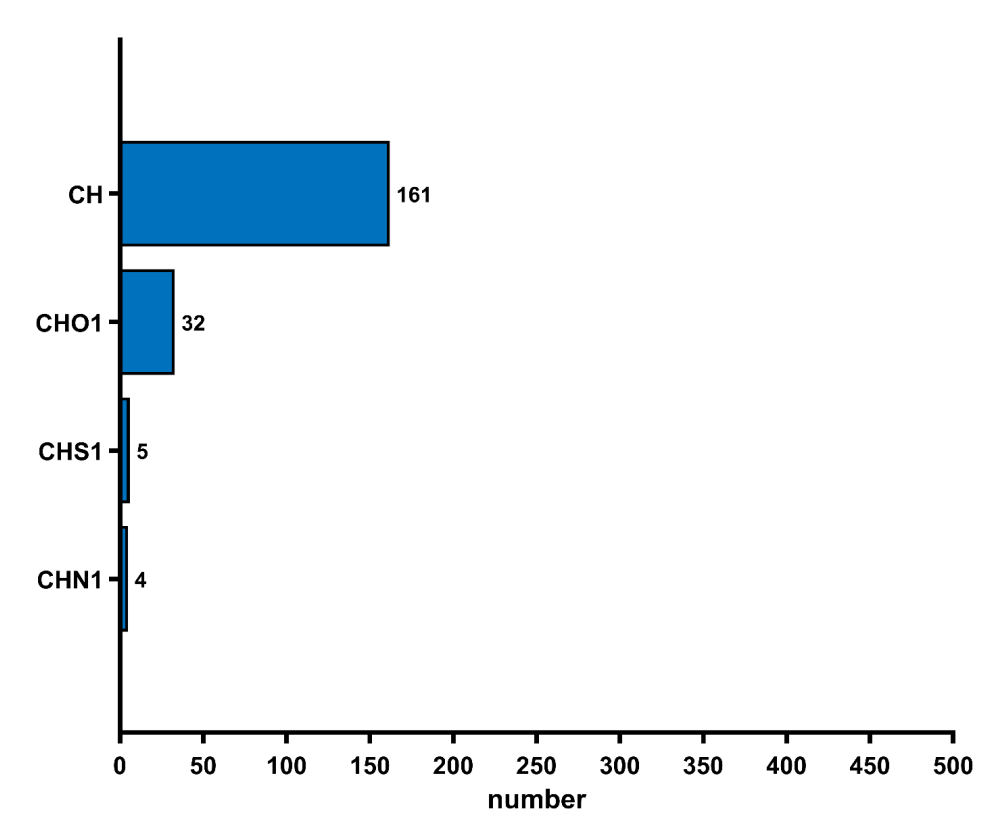


Figure S11: Compound class distribution of the diesel emissions. The displayed data are average chemical speciation from 5 min (540 scans) of stable emission conditions at 20 kW load.

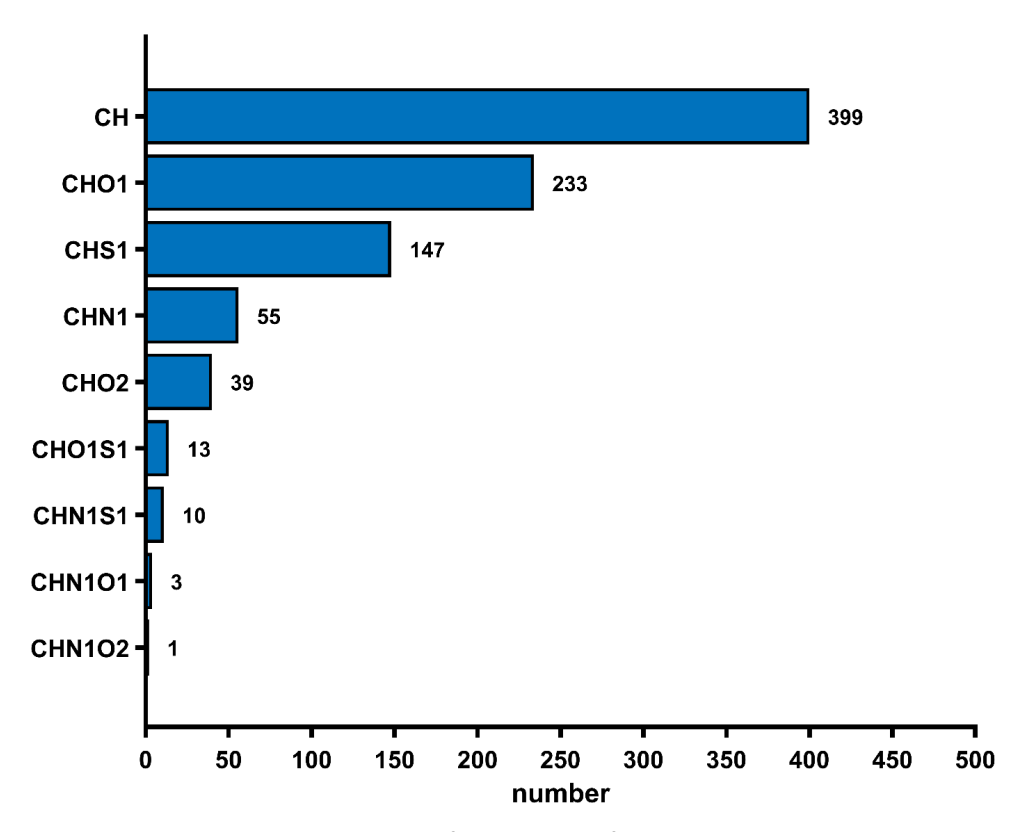


Figure S12: Compound class distribution of the heavy fuel oil emissions without scrubber. The displayed data are average chemical speciation from 5 min (540 scans) of stable emission conditions at 20 kW load.

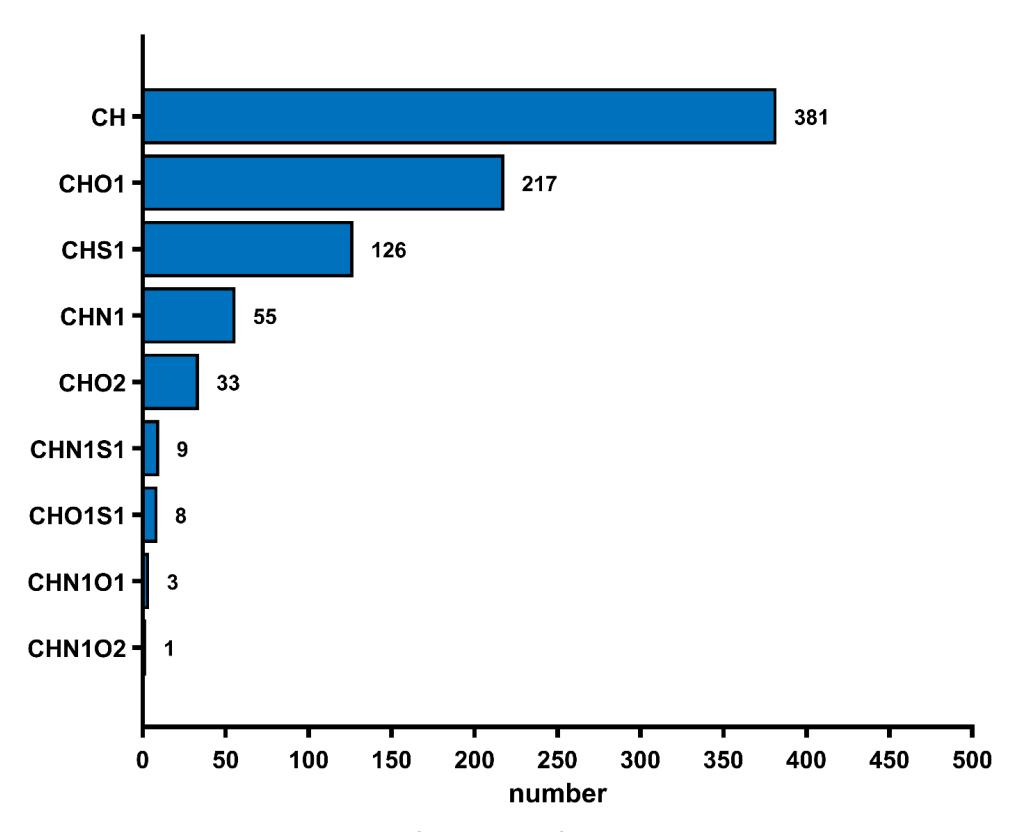


Figure S13: Compound class distribution of the heavy fuel oil emissions with scrubber. The displayed data are average chemical speciation from 5 min (540 scans) of stable emission conditions at 20 kW load.

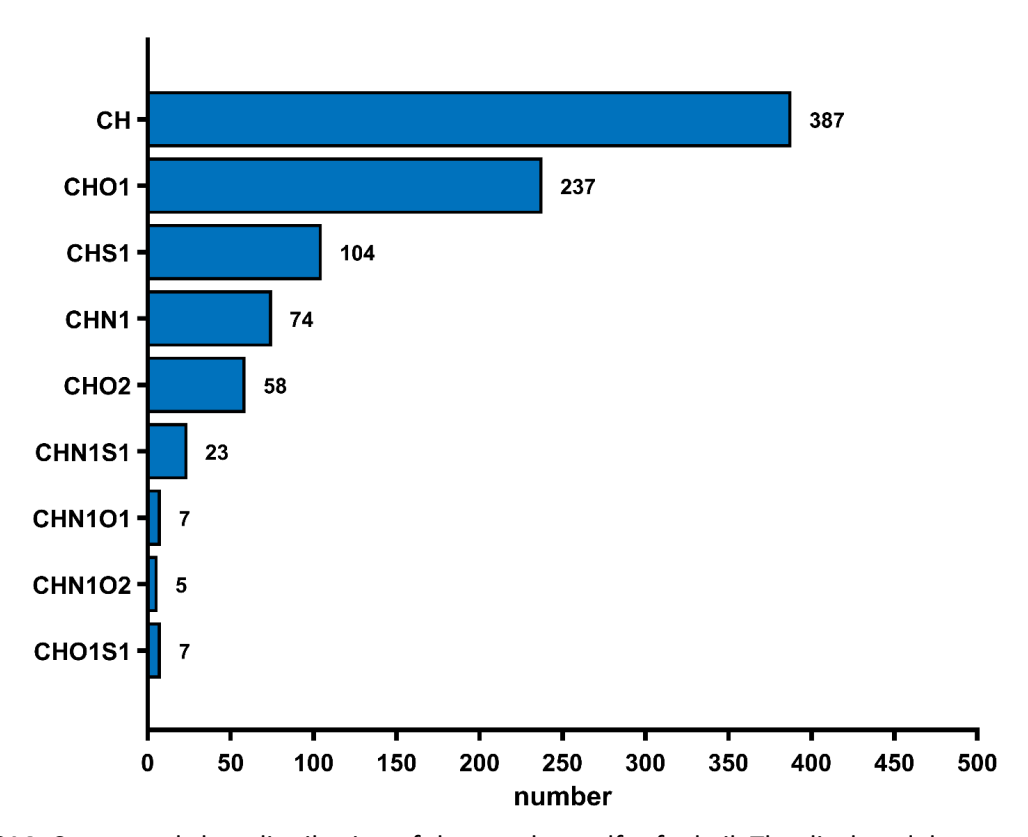


Figure S14: Compound class distribution of the very low sulfur fuel oil. The displayed data are average chemical speciation from 5 min (540 scans) of stable emission conditions at 20 kW load.

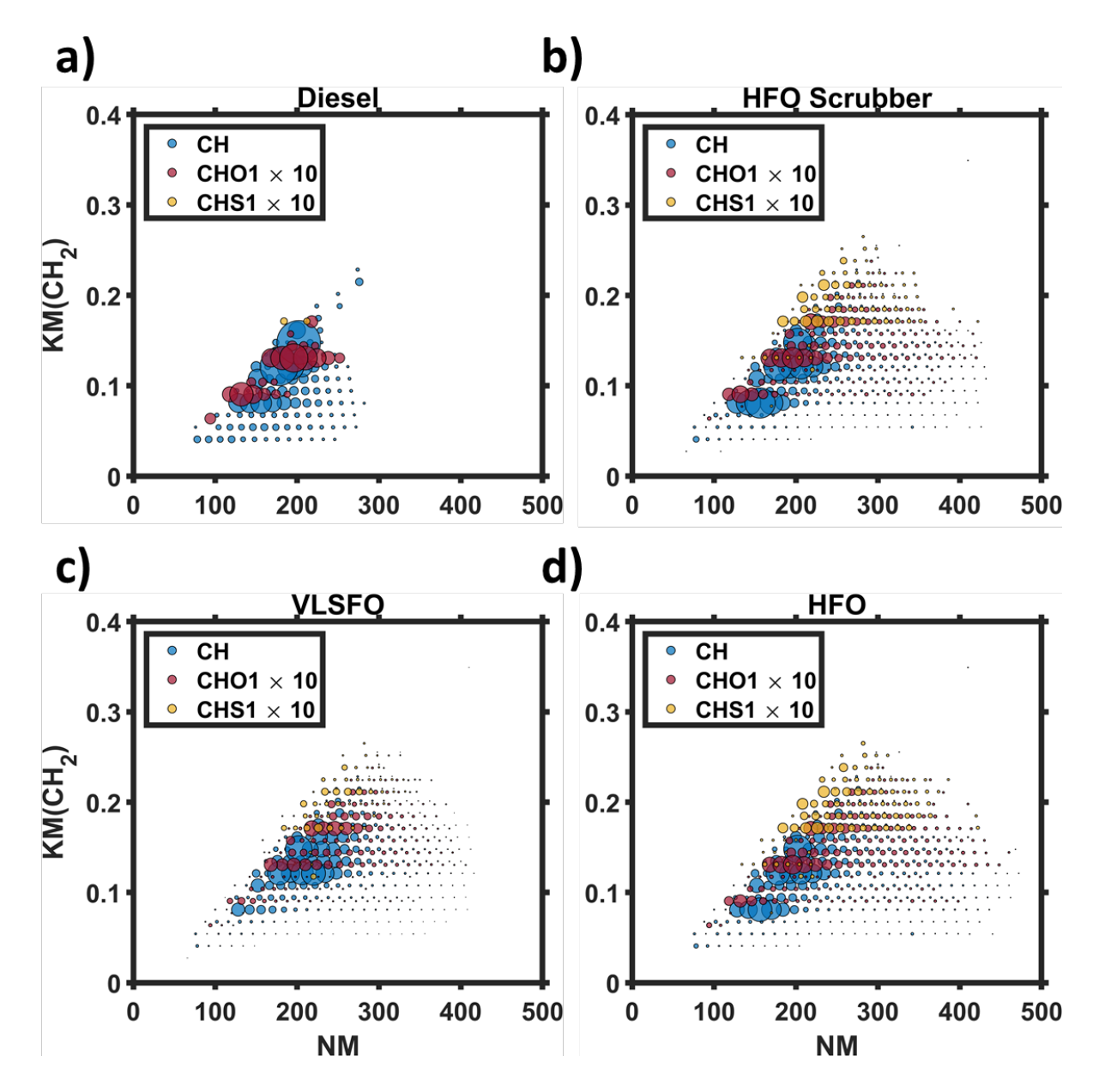


Figure S15: Kendrick mass defect plots for the mass increment CH₂. Compound classes are color-coded (blue – CH-, red – CHO-, and yellow – CHS-class). Please note that for visualization the size of the CHO- and CHS-class compounds is increased by a factor of 10. CHS-class relative contribution nicely correlates with fuel sulphur content (FSC). No significant effect was found comparing primary HFO gas emissions and HFO emissions after wet-scrubber exhaust gas treatment. Important for regulatory bodies, the VLSFO, despite being a low sulphur feed, exhibits a strong profile of unsaturated aromatic constituents with high mass defects. The nature of these alarming compounds released from an IMO 2020 permitted fuel can most likely be traced back to the cycle-oil (a cheap by-product in petroleum refining) content of the VLSFO.

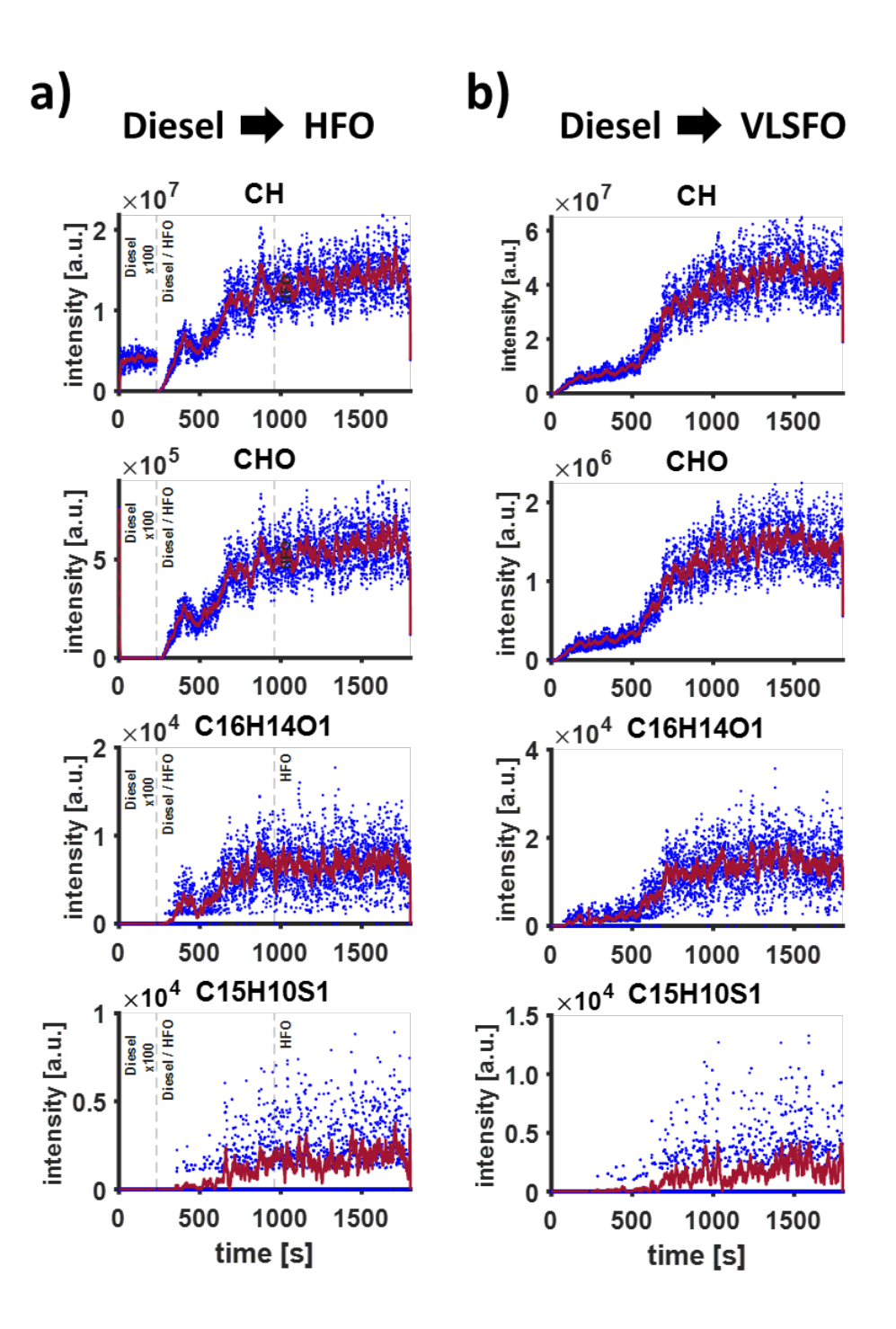


Figure S16: Extracted time-resolved traces for the CH- and CHO-class as well as the exemplary attributed elemental compositions $C_{16}H_{10}O_1$ (DBE 10) and $C_{15}H_{10}S_1$ (DBE 11) for the transmission from a) diesel to heavy fuel oil (HFO), with a stabilization at about 1,000 s, and b) diesel to very low sulfur fuel oil, stabilizing at roughly 1,200 s. For both cases, an overall increase for all traces is noticeable after change from distillate fuel towards a heavier feed.

References

- (1) Kösling, P.; Rüger, C. P.; Schade, J.; Fort, K. L.; Ehlert, S.; Irsig, R.; Kozhinov, A. N.; Nagornov, K. O.; Makarov, A.; Rigler, M.; Tsybin, Y. O.; Walte, A.; Zimmermann, R., Vacuum Laser Photoionization inside the C-trap of an Orbitrap Mass Spectrometer: Resonance-Enhanced Multiphoton Ionization High-Resolution Mass Spectrometry. *Anal Chem* **2021**, 93, 9418–9427, DOI: 10.1021/acs.analchem.1c01018.
- (2) Adam, T. W.; Clairotte, M.; Streibel, T.; Elsasser, M.; Pommeres, A.; Manfredi, U.; Carriero, M.; Martini, G.; Sklorz, M.; Krasenbrink, A.; Astorga, C.; Zimmermann, R., Real-time analysis of aromatics in combustion engine exhaust by resonance-enhanced multiphoton ionisation time-of-flight mass spectrometry (REMPI-TOF-MS): a robust tool for chassis dynamometer testing. *Anal Bioanal Chem* **2012**, 404, 273–276, DOI: 10.1007/s00216-012-6112-6.
- (3) Gehm, C.; Streibel, T.; Passig, J.; Zimmermann, R., Determination of Relative Ionization Cross Sections for Resonance Enhanced Multiphoton Ionization of Polycyclic Aromatic Hydrocarbons. *Applied Sciences* **2018**, 8, 1617, DOI: 10.3390/app8091617.
- (4) Hanley, L.; Zimmermann, R., Light and molecular ions: the emergence of vacuum UV single-photon ionization in MS. *Anal Chem* **2009**, 81, 4174–4182, DOI: 10.1021/ac8013675.
- (5) Streibel, T.; Zimmermann, R., Resonance-enhanced multiphoton ionization mass spectrometry (REMPI-MS): applications for process analysis. *Annual review of analytical chemistry* **2014**, 7, 361–381, DOI: 10.1146/annurev-anchem-062012-092648.
- (6) Boesl, U., Laser mass spectrometry for environmental and industrial chemical trace analysis. *J. Mass Spectrom.* **2000** (35), 289–304.
- (7) Hsu, C. S.; Lobodin, V. V.; Rodgers, R. P.; McKenna, A. M.; Marshall, A. G., Compositional Boundaries for Fossil Hydrocarbons. *Energy Fuels* **2011**, 25, 2174–2178, DOI: 10.1021/ef2004392.
- (8) Marshall, A. G.; Rodgers, R. P., Petroleomics: chemistry of the underworld. *Proc Natl Acad Sci U S A* **2008**, 105, 18090–18095, DOI: 10.1073/pnas.0805069105.